MIGRATION VELOCITY ANALYSIS USING RESIDUAL DIFFRACTION MOVEOUT IN THE PRE-STACK DEPTH DOMAIN

T. A. Coimbra, J. J. S. de Figueiredo, A. Novais, J. Schleicher, and S. Arashiro

email: *tgo.coimbra@gmail.com*

keywords: *velocity analysis, diffractions, pre-stack depth migration*

ABSTRACT

A major cause of diffracted seismic waves in the subsurface are nonsmooth structures of sizes in the same order of the wavelength. Since the wavefield can be meaningfully affected by the these nonsmooth structures, many important model features can be inferred from the diffracted wavefield which can help to improve the seismic image. We derive a methodology for migration velocity improvement and diffraction localization based on a moveout analysis of over- or undermigrated diffraction events in the depth domain. The method does not depend on any requirements apart from a fairly arbitrary initial velocity model as input. We demonstrate that the method can be applied in both the pre- or post-stack domains. For each iteration, the method provides an update to the velocity model and consequently to the diffraction locations. The algorithm is based on the focusing of remigration velocity rays from uncollapsed migrated diffraction curves. These velocity rays are constructed from a ray-tracing like approach applied to the image-wave equation for velocity continuation. After each pre-stack migration, the method has a very low computational cost, and the diffraction points are located automatically. We demonstrate the feasibility of our method using two synthetic nonzero-offset data examples.

INTRODUCTION

The potential of seismic diffraction for seismic processing is well-known. Many recent publications make use of diffractions for velocity estimation (Sava et al., 2005; Novais et al., 2008; Landa and Reshef, 2009), hydrocarbon reservoir interpretation (Tsingas et al., 2011) and super-resolution (Khaidukov et al., 2004). Even though many studies have been dedicated to investigate the role of diffraction signatures in seismic processing, many challenges still exist and must be overcome. Recently, Landa (2012) has raised some important questions related to the potential of diffraction signatures in seismic processing and interpretation. Although most of time, diffraction signatures show a signal weaker than most reflections, methods capable to separate diffractions from reflections exist (see, e.g., Fomel et al., 2007) and can be valuable for further development in seismic diffraction imaging. We agree with Landa (2012), who states that "if diffraction receives the attention it deserves, we will be able to see the invisible".

One particularly important point is that diffraction events contain more direct information on the seismic velocities than reflection events. While from the latter, velocity information can only be extracted making use of data redundancy, the focusing of a single diffraction event, once identified in the data or made visible with diffraction/reflection separation, already provides access to a velocity estimate.

In this work, we propose a method for velocity improvement and diffraction-point localization based on the choosing and picking of residual moveout of incorrectly migrated diffraction events in the depth domain. Coimbra et al. (2011) derived the post-stack version of this method and successfully applied it to a simple zero-offset data set. Coimbra et al. (2012) demonstrated that the method is capable of extracting a

high-quality velocity model from the realistic SIGSBEE 2B data set. Here, we extend their analysis to the prestack case using diffraction curves for nonzero-offset depth-migration. At low computational cost, the method uses an approximate velocity model as an input and provides an update.

We propose two algorithms for the use of the residual diffraction moveout for velocity updating. They are based on depth remigration (Hubral et al., 1996a,b; Tygel et al., 1996; Schleicher et al., 1997, 2004) and give rise to an automated method for diffraction location that relies on the picking of uncollapsed diffractions in the pre-stack migrated image. The feasibility of our method is shown through its application in two numerical examples.

METHOD AND THEORY

We extend the diffraction-imaging and velocity-updating method of Coimbra et al. (2011) to the prestack domain. Since the method makes use of the moveout of an incorrectly migrated diffraction in the depth domain, we start with deriving its expression for nonzero-offset.

Residual diffraction moveout

Consider a diffraction point at (x_d, z_d) in a constant-velocity medium with velocity v_d. Since a diffraction event migrated with the true velocity v_d focuses at the true position (x_d, z_d), its location after migration with a wrong velocity v_0 must be smeared over the Huygens image-wave (Hubral et al., 1996b). The Huygens image-wave is the curve or surface of all points where a possible (reflection or diffraction) event at a single image point might be placed when the migration velocity is changed. Fomel (2003) derives a short-offset approximation in the time domain. Substituting the vertical traveltime by $2z/v$, it can be represented in the depth domain as

$$z = \frac{v_0}{v_d}\sqrt{z_d^2 - \frac{v_d^2}{v_0^2 - v_d^2}(x - x_d)^2 + h^2\left(1 - \frac{v_d^2}{v_0^2}\right)}\,, \tag{1}$$

where h is the half-offset. Introducing the sign symbol $s = \text{sgn}(v_0^2 - v_d^2) = \text{sgn}(v_0 - v_d)$ of the difference between the true and migration velocities, this equation can be rewritten as an ellipse or hyperbola,

$$\frac{z^2}{b^2} + s\frac{(x - x_d)^2}{a^2} = 1\,, \tag{2}$$

where the half-axes a and b are given by

$$\begin{aligned} a &= \frac{\sqrt{|v_0^2 - v_d^2|}\sqrt{v_0^2(z_d^2 + h^2) - v_d^2h^2}}{v_d v_0}, \\ b &= \frac{\sqrt{v_0^2(z_d^2 + h^2) - v_d^2h^2}}{v_d}. \end{aligned} \tag{3}$$

For $h = 0$, these expressions reduce to the zero-offset versions of Coimbra et al. (2011).

As we can see from equation (2), when the migration velocity is smaller than the medium velocity, $s = -1$, i.e., the undermigrated diffraction event follows a hyperbola. On the other hand, when the migration velocity is higher than the medium velocity, we have $s = 1$, i.e., the overmigrated diffraction event follows an ellipse.

Basic velocity updating strategy

Whenever the local velocity distribution at the diffraction point is reasonably well approximated by a constant average velocity, we can use the theoretical description in equation (2) to pick the incorrectly migrated diffraction events. As described in Coimbra et al. (2011, 2012), we use the least-squares method to find the best-fitting hyperbola to describe an undermigrated diffraction event or the best-fitting ellipse for an overmigrated diffraction event. This provides estimates for the half-axes a and b as well as for horizontal coordinate of the apex, x_d.

Once we have estimates for a, b, and x_d, we can find corresponding estimates for the average medium velocity and diffractor depth. Solving equation system (3) for v_d and z_d, we find

$$v_d = v_0\sqrt{1 - s\frac{a^2}{b^2}} \qquad \text{and} \quad z_d = \sqrt{\frac{v_d^2}{v_0^2}(h^2 + b^2) - h^2}\ . \tag{4}$$

In practice, however, the curves are no perfect ellipses or hyperbolas. Therefore, the results depend on the size of the aperture in which the hyperbolae or ellipses are fitted to the migrated diffraction event. In our implementation, we chose the aperture that provided the best fitting.

Moreover, incorrectly migrated diffraction events in an environment with a very strong velocity gradient exhibit a strong tilt. For a better description of the residual moveout in this case, we modify equation (2). We use a mixed perturbation term $\epsilon(x-x_d)z$ to allow for a rotation of the ellipse or hyperbola, i.e., equation (2) becomes

$$\frac{z^2}{b^2} + s\frac{(x - x_d)^2}{a^2} = 1 + \epsilon(x - x_d)z\ . \tag{5}$$

The perturbation parameter ϵ is adjusted together with the other parameters of the ellipse or hyperbola in the least-squares procedure. Its value is not used in our present version of the velocity updating strategy.

Velocity updating using remigration trajectories

The above velocity-updating procedure has a practical drawback. It provides, for each identified and picked diffraction event, a single velocity estimate that is strongly dependent on the quality of the ellipse or hyperbola fitting, but gives no clue about the quality of the constant-velocity assumption or the velocity estimate.

There is a more sophisticated way of using the information contained in the residual diffraction moveout for a velocity updating procedure, which allows some quality control. It is based on the velocity continuation method, also known as image-wave equation for remigration. This is an imaginary continuation operation in which the seismic image is transformed continuously in the post-migration domain (Fomel, 1994, 2003; Hubral et al., 1996b; Sava and Fomel, 2003; Schleicher et al., 2004) as a function of velocity. Mathematically, it is described by a so-called image-wave equation. In the depth domain, this equation is given by

$$\frac{\partial^2 I}{\partial x^2} + \alpha(h,z)^2\frac{\partial^2 I}{\partial z^2} + \frac{v}{z}\frac{\partial^2 I}{\partial v \partial z} = 0\ , \tag{6}$$

where $I = I(x, z, v)$ is an image-wave function representing the seismic image to be transformed, x, z are the space variables, v is the average velocity at an image point (x, z) and

$$\alpha(h,z) = \sqrt{1 + h^2/z^2} \tag{7}$$

is an offset-depth dependent factor that reduces to one for zero offset. By applying a ray-theory-like approach to the remigration image-wave equation, ray-like trajectories can be found. These remigration trajectories are the set of positions where a selected reflection point can be found in a migrated image as a function of migration velocity.

Remigration trajectory tracing

In order to describe the kinematic part of depth remigration, we use an WKBJ or ray-theory-type approximation

$$I(x, z, v) = A(x, z)F(v - V(x, z)) \tag{8}$$

to represent the seismic image. In equation (8), F is the seismic wavelet, amplitude factor A represents the dynamic behavior, and V is image-wave eikonal describing the kinematic behavior of the image under variation of the migration velocity. Substituting expression (8) in image-wave equation (6) for depth remigration, we find that V must satisfy the image-eikonal equation

$$\left(\frac{\partial V}{\partial x}\right)^2 + \alpha(h,z)^2\left(\frac{\partial V}{\partial z}\right)^2 - \frac{V}{z}\frac{\partial V}{\partial z} = 0\ . \tag{9}$$

This image-eikonal equation is a nonlinear partial differential equation that can be solved by means of the method of characteristics (Courant and Hilbert, 1989). This method provides us with the characteristic trajectories along which image propagation takes place from one point (x, z) in the depth domain to another point (x_*, z_*), associated with a different migration velocity. It is these trajectories that we refer to as remigration trajectories.

In analogy to the development for the zero-offset case (Coimbra et al., 2011), we write equation (9) as a hyper-surface G given by

$$G(x, z, V, p, q) = p^2 + \alpha(h, z)^2 q^2 - \frac{V}{z} q = 0 \, , \tag{10}$$

where $p = \partial V/\partial x$ and $q = \partial V/\partial z$ are new variables. The method of characteristics then consists of transforming this hypersurface into the following system of ordinary differential equations

$$\begin{aligned}
\frac{dx}{dv} &= \lambda \frac{\partial G}{\partial p} = 2\lambda p \, , \\
\frac{dz}{dv} &= \lambda \frac{\partial G}{\partial q} = \lambda \left(2\alpha(h, z)^2 q - \frac{V}{z} \right) \, , \\
\frac{dp}{dv} &= -\lambda (G_x + p G_V) = \lambda \frac{qp}{z} \, , \\
\frac{dq}{dv} &= -\lambda (G_z + q G_V) = -\frac{\lambda}{z} \left(p^2 - \left(\alpha(h, z)^2 - 1 \right) q^2 \right) \, , \\
\frac{dV}{dv} &= \lambda (p G_p + q G_q) = \lambda \left(p^2 + \alpha(h, z)^2 q^2 \right) = 1 \, .
\end{aligned} \tag{11}$$

In the first five equations of system (11), v could be any monotonously increasing variable along the trajectory. The actual meaning of this variable is defined by the last equation in the above system. For convenience, we have imposed the meaning of the independent variable to be the (average) velocity by setting the derivative of the image-eikonal V with respect to v to one. This choice defines the scale factor λ as

$$\lambda = \left(p^2 + \alpha(h, z)^2 q^2 \right)^{-1} \, . \tag{12}$$

System (11) describes the remigration trajectories the image wave follows under variation of v. In other words, all variables involved in the propagation process are parameterized in terms of v, i.e., as $x = x(v)$, $z = z(v)$, $p = p(v)$, $q = q(v)$, and $V = V(v)$. For zero-offset ($h = 0$), the solution to system (11) are circular arcs (Schleicher et al., 1997). For non-zero-offset, they can be found using numerical ray tracing.

To make use of system (11) for the tracing of remigration trajectories, we need initial conditions for all of the involved variables. Let us assume that a remigration trajectory starts at an image-point (x_0, z_0) in an image I_0 obtained with velocity v_0. This defines the initial values for image-wave ray tracing as $x(v_0) = x_0$, $z(v_0) = z_0$ and $V(v_0) = v_0$. We still need the initial values $p(v_0) = p_0$ and $q(v_0) = q_0$. These can be found in analogous way as in the zero-offset case (Coimbra et al., 2011). For one, these values satisfy the image-eikonal equation (10) at $v = v_0$, i.e.,

$$p_0^2 + \alpha^2 q_0^2 - \frac{v_0}{z_0} q_0 = 0 \, , \tag{13}$$

where $\alpha_0 = \alpha(h, z_0)$. Equation (13) is equivalent to the elliptic expression

$$p_0^2 + \left(\alpha_0 q_0 - \frac{v_0}{2 z_0 \alpha_0} \right)^2 = \frac{v_0^2}{4 z_0^2 \alpha_0^2} \, . \tag{14}$$

Introducing a parameter θ, we can thus represent the relationship (14) between p_0 and q_0 as

$$p_0 = \frac{v_0 \sin(\theta)}{2 z_0 \alpha_0} \qquad \text{and} \qquad q_0 = \frac{v_0 (\cos(\theta) + 1)}{2 z_0 \alpha_0^2} \, . \tag{15}$$

The value of parameter θ that defines the correct trajectory at the initial point (x_0, z_0) in the original seismic event $I_0(v_0)$ is determined as follows. Along the initial seismic event, the image-wave eikonal must satisfy

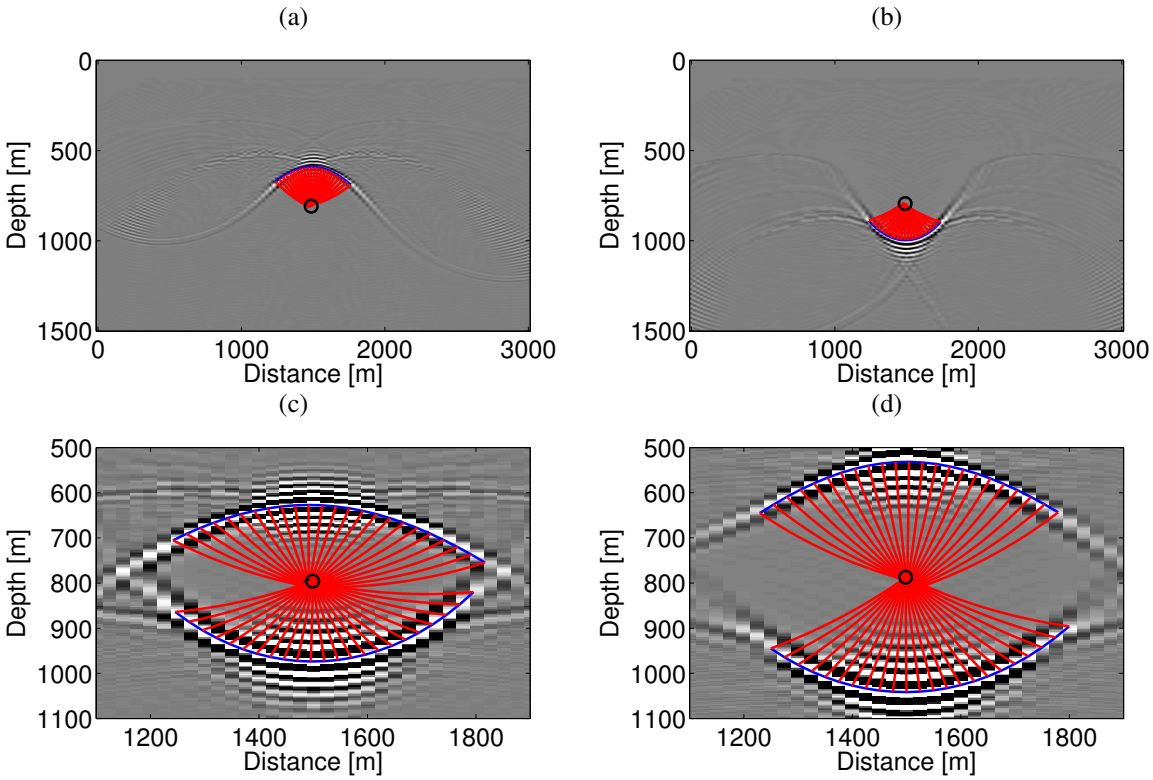

Figure 1: (a) Pre-stack migrated section ($h = 200$ m) with remigration trajectories (red lines) starting at an undermigrated hyperbolic diffraction curve (blue line). The black circle indicates the true diffractor position. (b) Pre-stack migrated section ($h = 200$ m) with remigration trajectories (red lines) starting at an overmigrated elliptic diffraction curve (blue line). (c) Superposition of center sections of parts a and b. The focusing of the remigration trajectories (red lines) at the correct point is independent of the original (wrong) migration velocity. The quality of the focussing is an indication for the quality of the velocity estimate. (d) Same as part c for half-offset $h = 600$ m.

$V(x, z(x)) = v_0$ or $dV/dx = 0$. Implicit derivation with respect to the horizontal coordinate x and solution for dz/dx yields

$$D_0 = \frac{dz}{dx} = -\frac{\partial V}{\partial x}\left(\frac{\partial V}{\partial z}\right)^{-1} = -\frac{p_0}{q_0} = -\frac{\alpha_0 \sin(\theta)}{\cos(\theta)+1}\,, \tag{16}$$

where D_0 is the dip of the migrated event at the initial point (x_0, z_0) of the remigration trajectory. Equation (16) can be inverted to yield the correct value of θ in dependence on the event dip,

$$\theta = -\arcsin\left(\frac{2D_0\alpha_0}{D_0^2+\alpha_0^2}\right)\,. \tag{17}$$

Substituting these expressions back in equations (15) yields

$$p_0 = -\frac{v_0}{z_0}\frac{D_0}{D_0^2+\alpha_0^2} \qquad \text{and} \qquad q_0 = \frac{v_0}{z_0}\frac{1}{D_0^2+\alpha_0^2}\,. \tag{18}$$

These two equations complete the set of initial conditions needed for the tracing of the remigration trajectories using system (11).

Figures 1 show examples of remigration trajectories (thin red lines) for an incorrectly migrated diffraction event. The trajectories focus at a point close to the true diffractor position. The point on each trajectory closest to the focus point (in the figure, the trajectories end at the focus point) provides an associated velocity value for that point. In this way, the residual moveout of the incorrectly migrated diffraction events

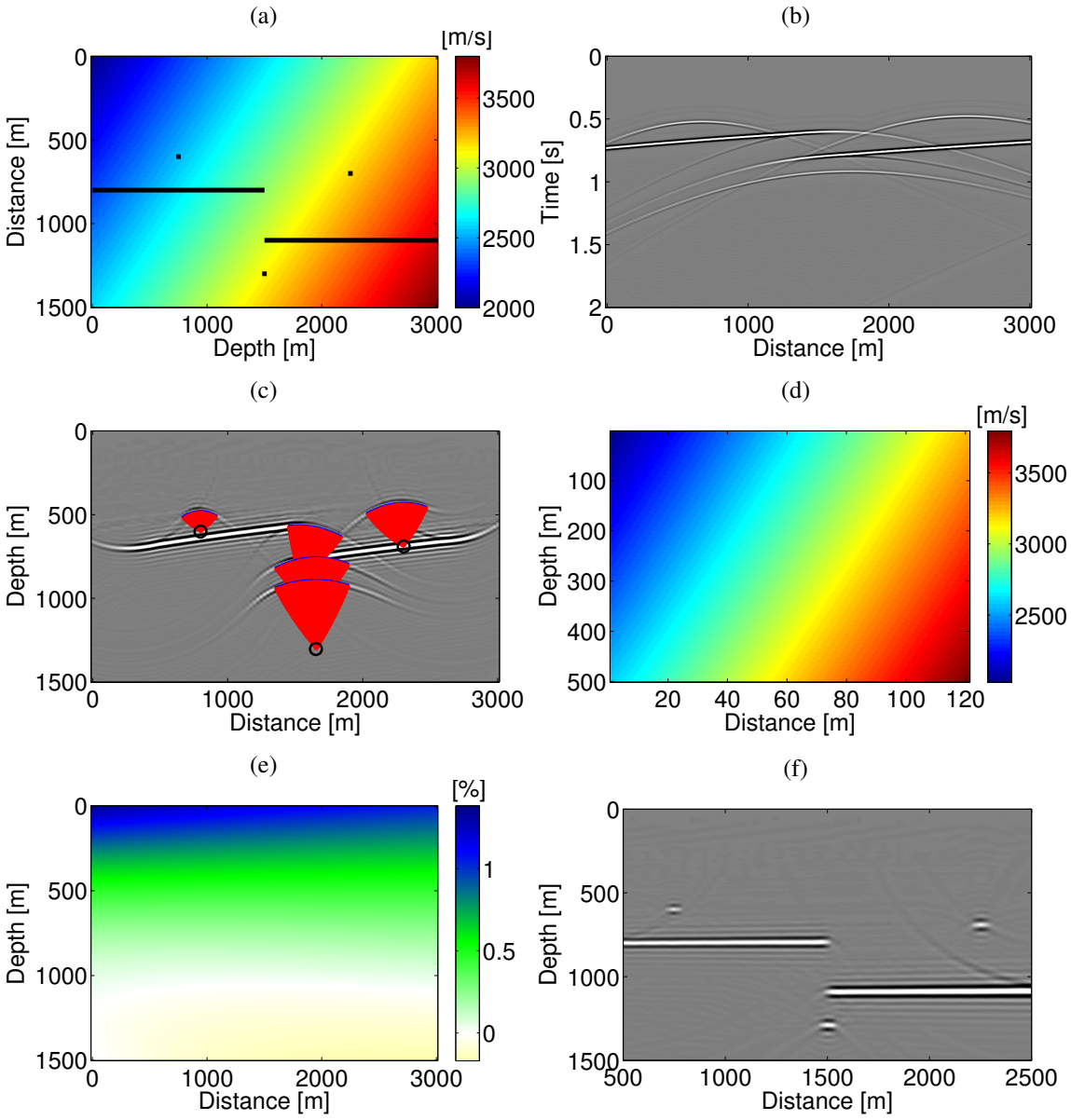

Figure 2: (a) Velocity model with constant diagonal gradient $v(x, z) = 2000 + 0.4x + 0.4z$ m/s. (b) Common-offset time section for $h = 200$ m. (c) Depth migrated image and undermigrated hyperbolas (blue lines) and focusing remigration trajectories (red lines). A constant velocity of 2000 m/s was used for migration. (d) The inverted interval velocity model. (e) Relative velocity error. (f) Migrated image using this interval velocity model.

can be used to update the migration velocity model. The focus-point scatter provides an indication for the quality of the velocity estimate.

RESULTS FOR TWO SYNTHETIC DATA SETS

Small offset

To investigate the quality of our method in the presence of lateral inhomogeneity, we applied it to data from a model with three diffraction points, buried in a constant-gradient velocity background with vertical and lateral variation, given by $v(x, z) = 2000 + 0.4x + 0.4z$ m/s (Figure 2a). It also contains two horizontal

reflector elements with endpoints in the center of the model. We used Kirchhoff modeling with a Ricker wavelet of dominant frequency 20 Hz to generate a common-offset dataset for a half-offsets $h = 200$ m. The acquisition geometry consisted of 300 source-receivers pairs spaced at 10 m, covering an extension of 3000 m. Figure 2b shows the resulting common-offset data.

We then depth-migrated these data using a constant velocity of 2000 m/s (Figure 2c). Of course, the reflectors are in wrong positions and the diffractions are not focused at all. We then fitted hyperbolas to the undermigrated diffractions (blue lines in Figure 2c) and traced the corresponding remigration trajectories (red lines in Figure 2c). The remigration trajectories focus almost exactly at the true diffractor positions. In this example, even under rather strong lateral and vertical velocity gradients, the method was capable of localizing all diffraction points with an error of $\pm 0.4\%$ in the vertical direction and up to $\pm 0.5\%$ in the horizontal direction.

We interpolated the resulting average velocity values using a linear least-squares fit to obtain a mean-velocity model given by $V_m(x, z) = 2044 + 0.38x + 0.18z$ m/s. To invert this mean velocity model for interval velocity, we use that depth remigration averages the slowness (Schleicher et al., 2004). The resulting inverted interval velocity model is $V_r(x, z) = 2044 + 0.38x + 0.37$ m/s. Figure 2d shows this inverted velocity model, and Figure 2e shows its relative error. The error amounts to less than 2% at the top of the model and is much lower in the center and at the bottom, where the actual velocity information is located.

Finally, Figure 2f shows a depth migrated section using the velocity model in Figure 2d. The migrated image focuses all three diffractions points in the model and correctly positions the two straight reflector elements. Note that for this small offset, a single iteration was sufficient to construct a suitable velocity model.

Larger offset

Next we repeated this experiment with a larger half-offset of $h = 600$ m, keeping all other parameters the same. With the same velocity model depicted at Figures 2a and again using zero-order Kirchhoff modeling, we generated a second common-offset panel for a half-offset of $h = 600$ m. Again, we migrated this panel using a constant velocity model of 2000 m/s. The result is shown in Figure 3a, which also depicts the fitted undermigrated hyperbolas (blue lines) and the corresponding remigration trajectories (red lines).

The first interval model from the inversion of the resulting average velocities is shown in Figure 3b, with its error depicted in Figure 3c. As we can see, the larger offset led to a larger error, amounting to almost 12% at the bottom of the model. This insufficient model reflects in the quality of the associated migrated image (Figure 3d). While the reflector elements are already quite well imaged, only the diffraction at the left-hand side looks acceptable. The diffractions at the right-hand side and bottom of the image are still out of focus, indicating that further model improvement is called for.

Consequently, we applied our method again to these uncollapsed diffractions. The fitted hyperbolas (blue lines) and focusing remigration trajectories (red lines) are shown in Figure 3e. The updated velocity values led to a new interval velocity model of $V_r(x, z) = 2035 + 0.42x + 0.39$ m/s (see Figure 3f). This model is now rather close to the true velocity model, as we observe from its relative error in Figure 3g, which remains below 2.5%.

Finally, the result of a depth Kirchhoff migration using this inverted velocity model is shown in Figure 3h. As we can see, the reflector elements are correctly positioned in depth and all diffractors are nicely focused at their true positions (compare to Figure 2a). Thus, even for a rather strong velocity gradient and a larger offset, the method converges to an acceptable velocity model in only two iterations.

CONCLUSIONS

We have extended the remigration-trajectories method of Coimbra et al. (2011, 2012) to the nonzero-offset domain. The method uses the moveout of unfocused diffraction events in a prestack migrated seismic section. The focusing of remigration trajectories originating from these events is used to determine the correct location of the diffractor and the associated velocity value. Our methodology does not require any information apart from a fairly arbitrary initial velocity model for an initial depth migration. Except for the migrations involved, the processing time of the method is very fast. Once the diffraction events are selected

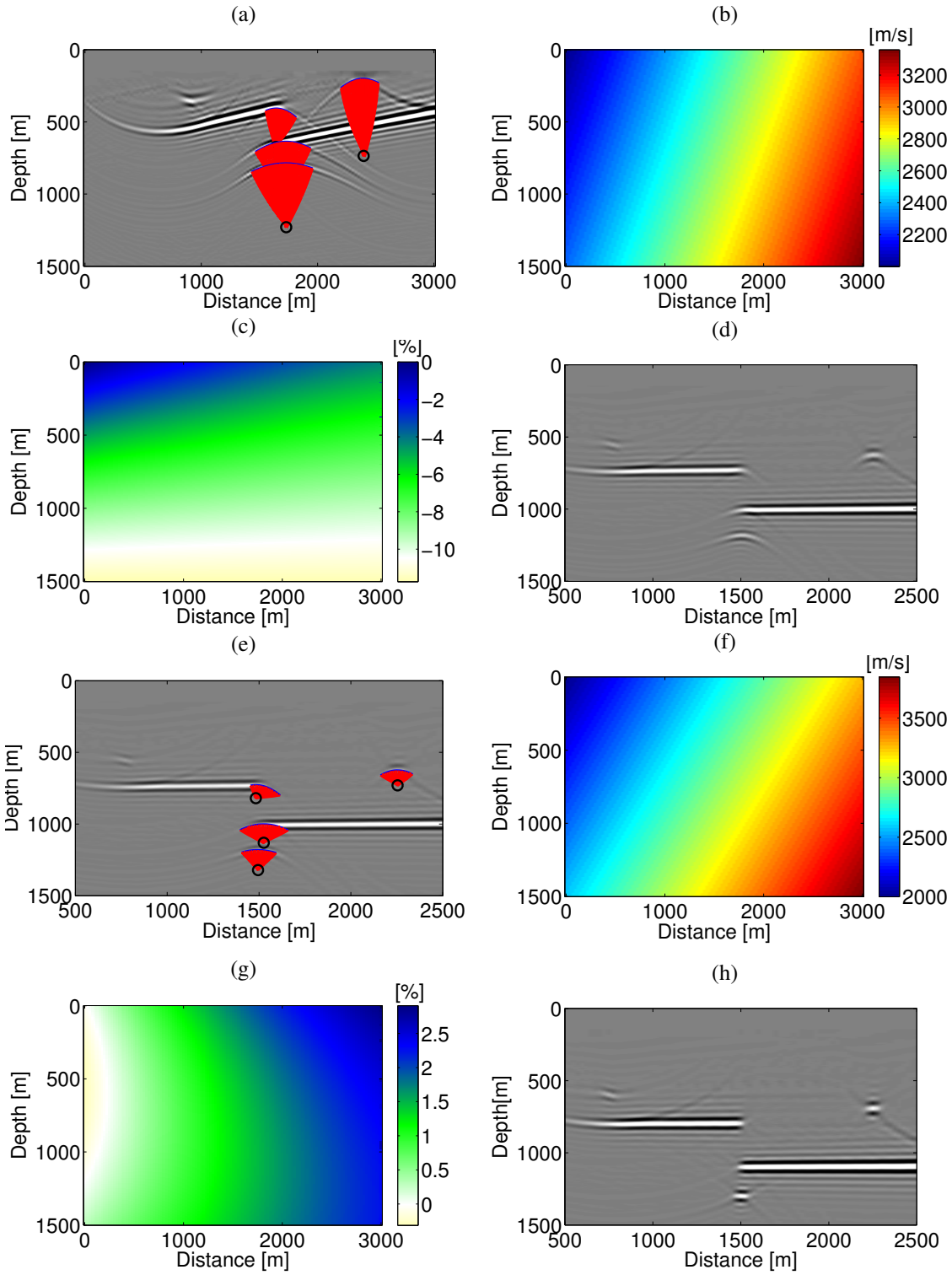

Figure 3: (a) Depth migrated image with constant velocity of 2000 m/s and with undermigrated hyperbolas (blue lines) and focusing remigration trajectories (red lines). (b) First interval velocity model resulting in $V_r(x, z) = 2055 + 0.35x + 0.19$ m/s. (c) Relative velocity error for first iteration. (d) The migrated image using the first interval velocity model. (e) The migrated image using the first interval velocity model and with undermigrated hyperbolas (blue lines) and focusing remigration trajectories (red lines). (f) Second interval velocity model. (g) Relative velocity error for second iteration. (h) The migrated image using the second interval velocity model.

and picked, the necessary computations are executed in a matter of seconds. We have tested the technique in a numerical model with a diagonal constant gradient. The method has worked satisfactorily. For a near offset ($h = 200$ m), only one iteration was required to obtain an acceptable velocity model with an error of less than 2%. All diffraction points were positioned with an error of less than 0.5%. For far-offset data ($h = 600$ m), two iterations were necessary to achieve the same quality.

ACKNOWLEDGEMENTS

This work was kindly supported by the Brazilian agencies CAPES, FINEP, and CNPq, as well as Petrobras and the sponsors of the Wave Inversion Technology (WIT) Consortium.

REFERENCES

Coimbra, T. A., de Figueiredo, J. J. S., Novais, A., and Schleicher, J. (2011). Migration velocity analysis with diffraction events using residual moveout. *Annual WIT report*, 15:57–70.

Coimbra, T. A., de Figueiredo, J. J. S., Schleicher, J., Novais, A., and Costa, J. C. (2012). Migration velocity analysis with diffraction events using residual moveout: Application to SIGSBEE 2B data. *Annual WIT report*, 16:45–58.

Courant, R. and Hilbert, D. (1989). *Methods of Mathematical Physics*, volume II. Wiley-Interscience.

Fomel, S. (1994). Method of velocity continuation in the problem of seismic time migration. *Russian Geology and Geophysics*, 35(5):100–111.

Fomel, S. (2003). Velocity continuation and the anatomy of residual prestack time migration. *Geophysics*, 68(5):1650–1661.

Fomel, S., Landa, E., and Taner, M. T. (2007). Poststack velocity analysis by separation and imaging of seismic diffractions. *Geophysics*, 72(6):U89–U94.

Hubral, P., Schleicher, J., and Tygel, M. (1996a). A unified approach to 3-D seismic reflection imaging - Part I: Basic concepts. *Geophysics*, 61(3):742–758.

Hubral, P., Tygel, M., and Schleicher, J. (1996b). Seismic image waves. *Geoph. J. Int.*, 125:431–442.

Khaidukov, V., Landa, E., and Moser, T. J. (2004). Diffraction imaging by focusing-defocusing: An outlook on seismic superresolution. *Geophysics*, 69(6):1478–1490.

Landa, E. (2012). Seismic diffraction: where's the value? In *82st Ann. Internat. Meeting, SEG, Expanded Abstracts*, pages 1–5.

Landa, E. and Reshef, M. (2009). Separation, imaging, and velocity analysis of seismic diffractions using migrated dip-angle gathers. In *79th Ann. Internat. Meeting, SEG, Expanded Abstracts*, pages 2176–2180.

Novais, A., Costa, J., and Schleicher, J. (2008). GPR velocity determination by image-wave remigration. *Journal of Applied Geophysics*, 65:65–72.

Sava, P., Biondi, B., and Etgen, J. (2005). Wave-equation migration velocity analysis by focusing diffractions and reflections. *Geophysics*, 70(3):U19–U27.

Sava, P. C. and Fomel, S. B. (2003). Angle-domain common image gathers by wavefield continuation methods. *Geophysics*, 68(5):1650–1661.

Schleicher, J., Hubral, P., Höcht, G., and Liptow, F. (1997). Seismic constant-velocity remigration. *Geophysics*, 62(2):589–597.

Schleicher, J., Novais, A., and Munerato, F. P. (2004). Migration velocity analysis by depth image-wave remigration: First results. *Geophysical Prospecting*, 52:559–573.

Tsingas, C., Marhfoul, B. E., Satti, S., and Dajani, A. (2011). Diffraction imaging as an interpretation tool. *First Break*, 29:57–61.

Tygel, M., Schleicher, J., and Hubral, P. (1996). A unified approach to 3-D seismic reflection imaging - Part II: Theory. *Geophysics*, 61(3):759–775.

APPENDIX

DERIVATION OF THE IMAGE-WAVE EQUATION

In this appendix, we derive the short-offset image wave equation (6) for remigration from equation (1). The procedure follows closely the lines of the zero-offset case of Hubral et al. (1996b). For simplicity, let us denote the ratio between the true and migration velocities by $M = v_0/v_d$. Then, we can rewrite equation (1) as

$$z^2 + h^2 = M^2(z_d^2 + h^2) - \frac{M^2(x - x_d)^2}{M^2 - 1} \,. \tag{19}$$

To derive the image-wave equation (6), we need to eliminate the unknown constants in equation (19) and replace them by derivatives. For this purpose, we have to assume that M is a function of x and z. Taking the derivatives of equation (19) with respect to x and z yields

$$0 = (z_d^2 + h^2)\frac{\partial M}{\partial x} + \frac{(x - x_d)^2}{(M^2 - 1)^2}\frac{\partial M}{\partial x} + \frac{M(x_d - x)}{M^2 - 1} \tag{20}$$

and

$$\frac{z}{M} = (z_d^2 + h^2)\frac{\partial M}{\partial z} + \frac{(x - x_d)^2}{(M^2 - 1)^2}\frac{\partial M}{\partial z} \,, \tag{21}$$

respectively. Combining equations (20) and (21), we obtain the auxiliary equation

$$\frac{M^2}{M^2 - 1}(x - x_d) = z\frac{\partial M}{\partial x}\left(\frac{\partial M}{\partial z}\right)^{-1} \,. \tag{22}$$

Together, these equations can now be used to eliminate x_d and z_d from equation (19). We find

$$\frac{z}{M}\frac{\partial M}{\partial z} = \left(\frac{z^2 + h^2}{M^2}\right)\left(\frac{\partial M}{\partial z}\right)^2 + \left(\frac{z}{M}\frac{\partial M}{\partial x}\right)^2 \,. \tag{23}$$

Substituting $M = V/v_d$, where $V = V(x, z)$ is the image-wave eikonal, we arrive at the image-eikonal equation

$$\left(\frac{\partial V}{\partial x}\right)^2 + \left(1 + \frac{h^2}{z^2}\right)\left(\frac{\partial V}{\partial z}\right)^2 - \frac{V}{z}\frac{\partial V}{\partial z} = 0 \,. \tag{24}$$

This equation justifies the image-wave equation (1), because that equation can be interpreted as the simplest second-order differential equation the kinematics of which is described by equation (24) upon the ansatz $I(x, z) = A(x, z)F(v - V(x, z))$.